Climate Dynamics (2019) 53:2557–2572
https://doi.org/10.1007/s00382-019-04641-3

Classifying past climate change in the Chew Bahir basin, southern Ethiopia, using recurrence quantification analysis

Martin H. Trauth[1] · Asfawossen Asrat[2] · Walter Duesing[1] · Verena Foerster[3] · K. Hauke Kraemer[1,4] · Norbert Marwan[4] · Mark A. Maslin[5] · Frank Schaebitz[3]

Received: 20 August 2018 / Accepted: 20 January 2019 / Published online: 2 February 2019

Abstract
The Chew Bahir Drilling Project (CBDP) aims to test possible linkages between climate and evolution in Africa through the analysis of sediment cores that have recorded environmental changes in the Chew Bahir basin. In this statistical project we consider the Chew Bahir palaeolake to be a dynamical system consisting of interactions between its different components, such as the waterbody, the sediment beneath lake, and the organisms living within and around the lake. Recurrence is a common feature of such dynamical systems, with recurring patterns in the state of the system reflecting typical influences. Identifying and defining these influences contributes significantly to our understanding of the dynamics of the system. Different recurring changes in precipitation, evaporation, and wind speed in the Chew Bahir basin could result in similar (but not identical) conditions in the lake (e.g., depth and area of the lake, alkalinity and salinity of the lake water, species assemblages in the water body, and diagenesis in the sediments). Recurrence plots (RPs) are graphic displays of such recurring states within a system. Measures of complexity were subsequently introduced to complement the visual inspection of recurrence plots, and provide quantitative descriptions for use in recurrence quantification analysis (RQA). We present and discuss herein results from an RQA on the environmental record from six short (< 17 m) sediment cores collected during the CBDP, spanning the last 45 kyrs. The different types of variability and transitions in these records were classified to improve our understanding of the response of the biosphere to climate change, and especially the response of humans in the area.

Keywords Paleoclimate dynamics · Eastern Africa · Pleistocene · Holocene · Time-series analysis · Recurrence plot

1 Introduction

The development by humans of settlement systems, artistic representations, and hunting strategies during the last 50–40 kyrs marks a "human revolution" and the emergence of behaviorally modern humans in Africa (Renfrew 2009; Richter et al. 2012). These behaviorally modern humans may have adapted to environmental changes and extreme climatic oscillations through technological, behavioural, cultural and cognitive innovation rather than through physical adaptation (Klein 1995; Klein and Steele 2013; Clark et al. 2016). Determining the nature and pace of changes in the environment of early modern humans is crucial to understanding the factors that influenced this human revolution. For example, different types of climate variability would have resulted in different types of climatic stress and changes to environmental boundaries (Hildebrand and Grillo 2012; Vogelsang and Keding 2013; Foerster et al. 2015).

There are currently ongoing discussions concerning global and regional climate fluctuations that had an effect on human habitats (e.g. Trauth et al. 2007, 2018; Foerster et al. 2015; Lamb et al. 2018; Ivory and Russell 2018; Maley et al. 2018; Garcin et al. 2018) and which did not, either because these fluctuations had little or no effect on the African climate (e.g. Timmerman and Friedrich 2016) or because their

✉ Martin H. Trauth
trauth@uni-potsdam.de

[1] Institute of Geosciences, University of Potsdam, Potsdam, Germany

[2] School of Earth Sciences, Addis Ababa University, Addis Ababa, Ethiopia

[3] Institute of Geography Education, University of Cologne, Cologne, Germany

[4] Potsdam Institute for Climate Impact Research, Potsdam, Germany

[5] Department of Geography, University College London, London, UK

effect was buffered by the environmental system (e.g. Cuthbert et al. 2017). Among the most debated episodes of African climate (including their onset, termination, and internal variability) are the Dansgaard–Oeschger (DO) cycles and Heinrich Events (HEs) (~ 110–12 kyr BP, e.g. Brown et al. 2007; Garcin 2008; Tierney and deMenocal 2013; Berke et al. 2014; Timmerman and Friedrich 2016; Lamb et al. 2018), the marine isotope stage 4 (MIS 4) aridification (~ 71 kyr BP, e.g. Timmerman and Friedrich 2016), the Last Glacial Maximum (LGM, 23.5–18 kyr BP, e.g. Gasse 2000; Shakun and Carlson 2010; Tierney and deMenocal 2013), and the African Humid Period (AHP, ~ 15–5 kyr BP, e.g. deMenocal et al. 2000; Tierney and deMenocal 2013; Shanahan et al. 2015; Tierney et al. 2017). Such global (DO cycles, HEs, LGM) and regional (AHP) episodes may have affected the availability of water and food, spatial retreats and shelter, and migration corridors, over variable periods of time (e.g. Ambrose 1998; Carto et al. 2009; Castañeda et al. 2009; Brandt et al. 2012; Foerster et al. 2015; Flohr et al. 2016; Marchant et al. 2018).

Time-series analysis provides a number of tools with which to characterize past climate change, which can be random, clustered, cyclic, or chaotic (e.g. Marwan et al. 2007; Mudelsee 2014; Trauth 2015). The most popular methods for characterizing variations are based on Fourier or wavelet transforms, decomposing time series into a linear combination of sinusoids (e.g. Trauth 2015 and references therein). Past climate change is, however, often nonlinear (i.e. there is no simple proportional relation between cause and effect) and techniques to describe nonlinear behavior have therefore become increasingly popular in recent decades, defining the scaling laws and fractal dimensions of natural processes (Kantz and Schreiber 1997; Turcotte 2010; Tsonis 2018) and detecting nonlinear interrelationships using methods such as transfer entropies, graphic models, and recurrence plots (Zbilut and Webber 1992; Marwan et al. 2003; Rodó and Rodríguez-Arias 2006; Feldhoff et al. 2013; Goswami et al. 2013; Runge et al. 2012, 2014; Builes-Jaramillo et al. 2018; Ramos et al. 2018). The availability of long time series in the Earth sciences in recent times (for example from multi-sensor core logger and micro X-ray fluorescence results) facilitates the use of these methods and increases the reliability of the results obtained.

In this paper we present a classification of past climate variability in the Chew Bahir basin of southern Ethiopia over approximately the last 45 kyrs using recurrence plots, which provide a graphic display of recurring states in the environmental system (Eckmann et al. 1987; Marwan et al. 2007). Quantitative descriptions (measures of complexity) have been developed to complement visual inspection of recurrence plots (RPs) and for recurrence quantification analysis (RQA) (e.g. Zbilut and Webber 1992; Marwan et al. 2007; Marwan 2008). We previously used recurrence plots to identify past climate transitions during the Plio-Pleistocene in Africa, the Middle East, and East Asia (e.g., Donges et al. 2011; Eroglu et al. 2016). Such plots enable us to detect nonlinear patterns in past climate change, helping to improve our understanding of the underlying process of climate transitions in the Chew Bahir basin by statistically describing the dynamical characteristics of the environment (Marwan et al. 2007, 2013; Donges et al. 2011; Marwan and Kurths 2015; Eroglu et al. 2016). We first used the method on prototypical data in order to assess its performance with typical palaeoclimate transitions. We then performed an RQA on the Late Quaternary climate record from Chew Bahir cores CB01–06 because it provides one of the most detailed records of climate change available from the vicinity of important sites for modern human fossil (Foerster et al. 2012, 2015, 2018; Trauth et al. 2015, 2018).

2 Regional setting

The sediment cores described herein were recovered from the Chew Bahir basin in the southern Ethiopian Rift (4.1–6.3°N, 36.5–38.1°E; Fig. 1) (see details in Foerster et al. 2012). Chew Bahir is a closed basin, separated from the Turkana Basin to the west by the Hammar Range. The western part of the 32,400 km^2 catchment, drained by the perennial Segen and Weyto rivers, is mostly formed by Late Proterozoic gneisses, whereas the eastern part is dominated by Miocene basalts (Moore and Davidson 1978; Davidson 1983). Rainfall in the area is associated with the seasonal migration of the Intertropical Convergence Zone (ITCZ), resulting in two rainy seasons in March–May and October–November (Nicholson 2017). Rainfall intensity strongly depends on Atlantic and Indian Ocean sea-surface temperature (SST) variations caused by the Indian Ocean Dipole (IOD) and the El Niño-Southern Oscillation (ENSO), also explaining the recent reduction of rainfall intensities over the last decades (Saji et al. 1999; Seleshi and Zanke 2004; Cheung et al. 2008; Segele et al. 2009; Nicholson 2017).

3 Methods

3.1 The Late Pleistocene–Holocene record of the Chew Bahir basin

We reconstructed climate fluctuations in the Chew Bahir from six short (< 17 m) sediment cores (CB01–06), collected along a ~ 20 km transect from Northwest to Southeast in the basin (Foerster et al. 2012, 2015; Trauth et al. 2018) (Fig. 1). These six cores were collected in a pilot study for the Hominin Sites and Paleolakes Drilling Project (HSPDP; HSPDP-CHB deep coring site in Fig. 1) (Cohen

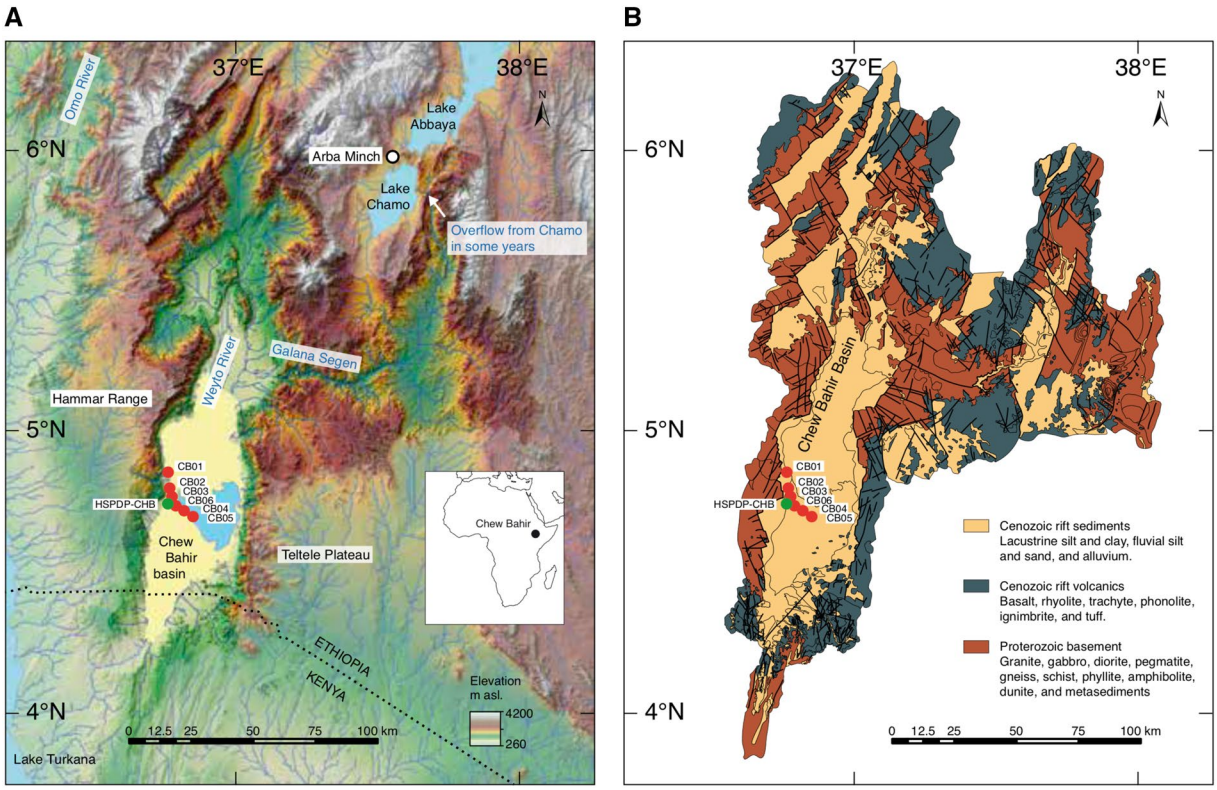

Fig. 1 **a** Topographic map of the Chew Bahir basin, showing the outline of the catchment, the drainage network, the locations of the short cores in the pilot study (2009, 2010), and the 2014 HSPDP-CHB drill site. **b** Geologic map of the Chew Bahir basin, showing the three generalized rock types: Cenozoic rift sediments, Cenozoic rift volcanics, and Proterozoic basement. Compilation based on Omo River Project Map (Davidson 1983), Geology of the Sabarei Area (Key 1988), Geology of the Yabello Area (Hailemeskel and Fekadu 2004), and Geology of the Agere Maryam Area (Hassen et al. 1997). Maps are modified versions of the ones previously published in Trauth et al. (2018) and Foerster et al. (2018)

et al. 2016; Campisano et al. 2017) and the Collaborative Research Center CRC-806 at the University of Cologne, and were described in detail in earlier publications (e.g., Foerster et al. 2012, 2015; Trauth et al. 2015). We used the potassium (K) concentrations of the sediment, determined by micro X-ray fluorescence (μXRF) scanning, as a proxy of aridity (Foerster et al. 2012, 2018; Trauth et al. 2015). Dynamic time warping (DTW) was employed for aligning the K records from the six cores CB01–06 (Trauth et al. 2018). The composite age model of Trauth et al. (2015), based on 32 AMS ^{14}C ages derived from biogenic carbonate, fossilized charcoal and organic sediment, resulting in a very solid chronology for lake record spanning the last ~ 45 kyr, was then used to convert composite core depths into ages.

A principal component analysis (PCA) helped us to separate the mixed regional and local environmental signals in the K records from the six aligned cores. The first principal component (PC1) contains more than 94% of the variance of the data and was therefore interpreted to best represent regional climate. The temporal resolution of the climate proxy record in CB01, with 2812 original measurements, has a calculated mean spacing of ~ 16 yrs, ranging from ~ 4 yrs in the upper part of the core to almost 2 kyrs in the deeper part of the core (Foerster et al. 2012, 2015; Trauth et al. 2015). The K record (following DTW alignment of cores CB01 to CB06 and PCA-based unmixing) runs from 45.358 to 0 kyr BP with a mean resolution of 8 yrs (ranging from 2.6 to 30.6 yrs) and the record has therefore been interpolated to an evenly-spaced time axis running from 45.358 to 0 kyr BP at 10 year intervals, which is close to the mean intervals of the original data (~ 16 yrs, ranging from ~ 4 yrs to 2 kyrs) and in the aligned and unmixed data (~ 8 yrs, ranging from 2.6 to 30.6 yrs) (Trauth et al. 2018).

3.2 Principles of recurrence plots (RPs) and recurrence quantification analysis (RQA)

We consider the Chew Bahir palaeolake to represent a complex system of interacting components, such as the waterbody, the sediment beneath the lake, and the organisms living within and around the lake. Systems with properties that change over time, such as the Chew Bahir palaeolake with its

slowly changing geomorphologic features, much more rapidly varying climatic factors, and the possible (very recent) influence of human activities, are known as dynamical systems. The Chew Bahir multi-dimensional palaeolake system is affected by a number of factors (known as *state variables* of the system) such as precipitation (with higher rainfall resulting in increased weathering and erosion within the catchment, and hence more potassium washed into the lake), evaporation (with increased evaporation producing more extreme hydrochemical conditions that enhance potassium fixation in the sediment through authigenic clay-mineral alterations, Foerster et al. 2012, 2018) and wind speed (with higher wind speeds and reduced vegetation cover resulting in more potassium-rich particles being blown into the lake).

Analysis of temporal variations in the state variables of the Chew Bahir palaeolake requires a record of the variables influencing those state variables over a relevant time period. Since the state variables of the Chew Bahir system (e.g., precipitation, evaporation and wind speed) cannot be measured directly, we use indirect indicators (known as climate proxies) measured from natural archives of environmental change such as the sediments of the Chew Bahir basin, sampled by coring. A proxy record of a multi-dimensional dynamical system obtained by sampling a single variable is equivalent to projecting the dynamics of a complex system onto a single axis (Iwanski and Bradley 1998). In our case the sampled variable is the series $x(t)$ of potassium concentrations x along a lake sediment core, which provides a natural archive of past influences on the Chew Bahir lake system, with sediment depth d converted into time t using the age model from Trauth et al. (2015).

One way to untangle the dynamics of a multi-dimensional system from a one-dimensional time series $x(t)$ is by time-delay embedding, which preserves the dynamic characteristics of the system (Packard et al. 1980) (Fig. 2). The reason why an entire system needs to be reconstructed from a single variable is that information about the system and the factors affecting its state variables is contained in a one-dimensional time series. In other words, since the potassium concentration in the Chew Bahir sediments is the result of a complex interplay between unknown amplitudes of different environmental (or state-) variables (such as precipitation, evaporation, and wind velocity), an analysis of the temporal variations in this environmental proxy will help us to understand the state variables of the Chew Bahir palaeolake and the time-varying interactions between its different components. The embedding of the time series $x(t)$ in a three-dimensional ($m=3$) coordinate system (a phase space), for example, means that three successive values $x(t)$, $x(t+\tau)$, and $x(t+2\tau)$ with a temporal separation of τ are represented by a single point within the phase space (Iwanski and Bradley 1998; Webber and Zbilut 2005; Marwan et al.

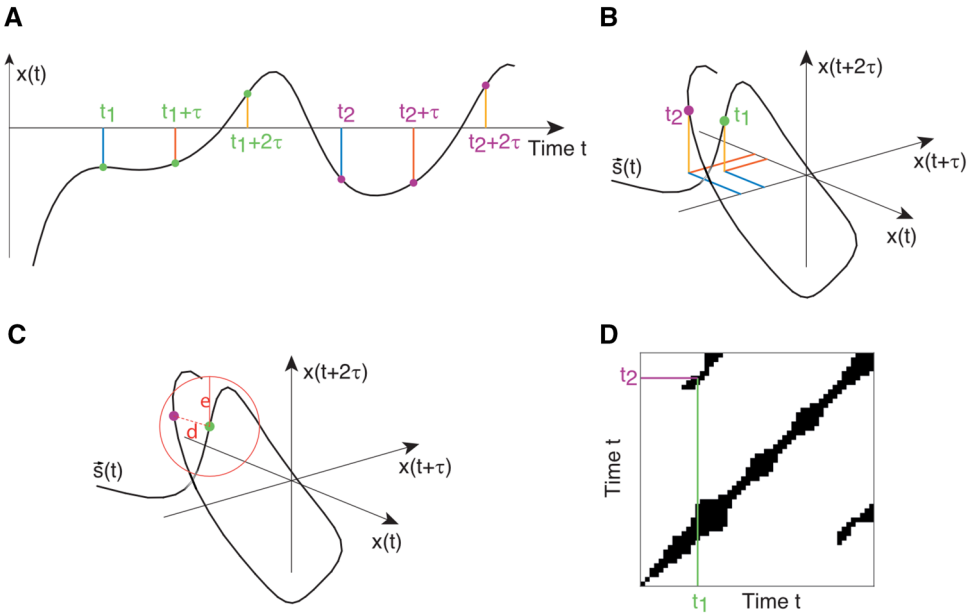

Fig. 2 Principle of recurrence plot. To untangle the dynamics of a multi-dimensional system from a onedimensional time series $x(t)$ (black line, in **a**) is by time-delay embedding. The embedding of the time series $x(t)$ in a three-dimensional ($m=3$) coordinate system (a phase space, shown in **b**), for example, means that three successive values $x(t)$, $x(t+\tau)$, and $x(t+2\tau)$ with a temporal separation of τ are represented as a single point $\vec{s}(t)$ within the phase space (Iwanski and Bradley 1998; Webber and Zbilut 2005; Marwan et al. 2007). Recurrence plots (RPs, **d**), first introduced by Eckmann et al. (1987), are graphic displays of such recurring states within a system, calculated from the distance (e.g. the Euclidean distance d, shown in **c**) between all pairs of phase space vectors $\vec{s}$ (t_1) and $\vec{s}$ (t_2), below a threshold value e (also shown in **c**) (Marwan et al. 2007)

2007) (Fig. 2). The geometric representation of the embedded time series of observations as trajectories $\vec{s}(t)=[x(t), x(t+\tau), x(t+2\tau)]$ within the phase space is called a phase portrait. The reconstructed phase space is not exactly the same as the original phase space, but its topological properties are preserved provided that the embedding dimension is sufficiently large (Packard et al. 1980; Takens 1981).

A common feature of dynamical systems is the property of recurrence (Webber and Zbilut 2005). Recurring patterns in the state of a system are a reflection of typical characteristics of the dynamical system. Defining these patterns can contribute significantly to our understanding of the system's dynamics. Changes in environmental (or state-) variables (such as precipitation, evaporation, and wind velocity) often follow characteristic courses (represented as trajectories $\vec{s}$ in phase space) that could lead to similar (but not identical) lake characteristics (e.g. depth and area of the lake, alkalinity and salinity of the lake, species assemblage in the waterbody, or formation of authigenic minerals in the sediment). Recurrence plots (RPs), first introduced by Eckmann et al. (1987), are graphic displays of such recurring states within a system, calculated from the distance (e.g. the Euclidean distance) between all pairs of phase space vectors $\vec{s}(t_1)$ and $\vec{s}(t_2)$, below a threshold value e (Marwan et al. 2007) (Figs. 2, 3).

Measures of complexity were subsequently introduced to complement the visual inspection of recurrence plots, providing quantitative descriptions for use in recurrence quantification analysis (RQA) (e.g. Zbilut and Webber 1992; Marwan et al. 2007; Marwan 2008). Among these, a selection of recurrence characteristics are very useful to summarize the appearance of the recurrence plots, ultimately helping to describe the behavior of the Chew Bahir lake system. An example of such a characteristic is the *recurrence rate* (*RR*),

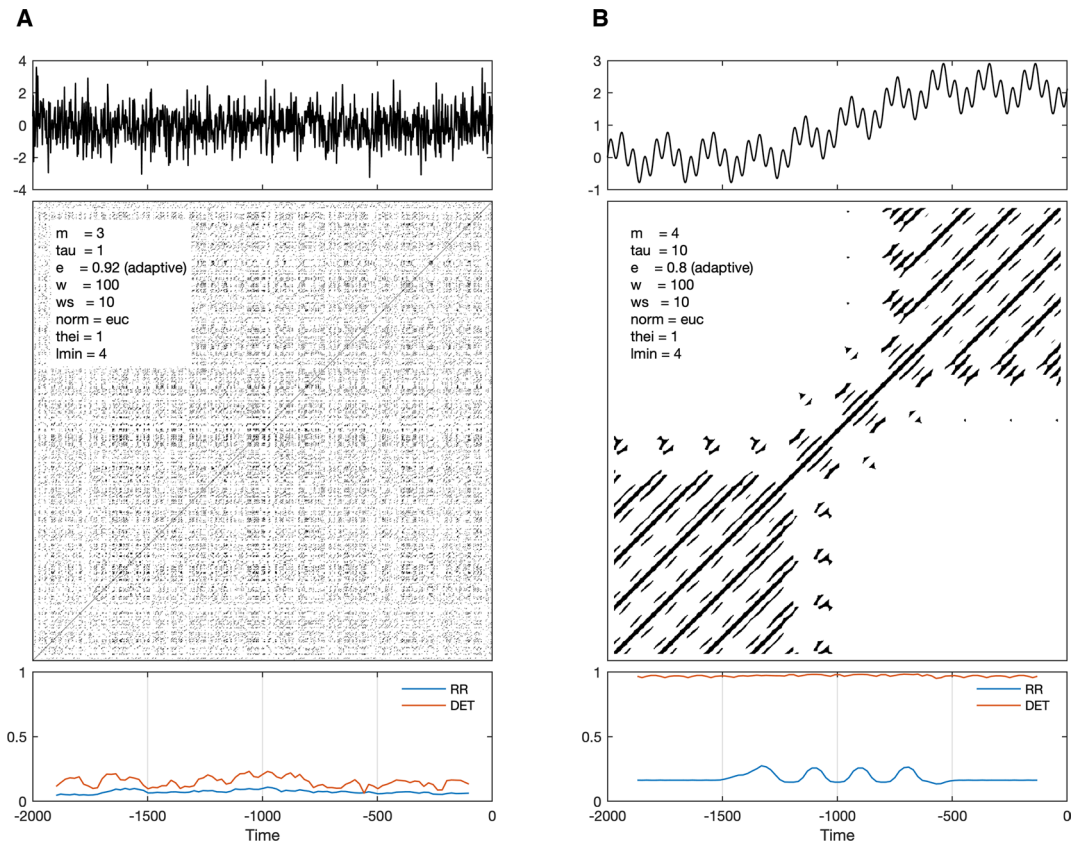

Fig. 3 **a**–**f** Recurrence plots (RPs) and recurrence quantification analysis (RQA) measures for synthetic data representing common types of dynamic behavior: **a** normally-distributed (Gaussian) noise. **b** Composite signal comprising two sine waves and a positive trend in the mean. **c** Composite signal comprising a sine wave and Gaussian noise with decreasing signal-to-noise ratio from left to right. **d** Composite signal comprising two sine waves and a trend in the frequencies. **e** Abrupt transition from a composite signal comprising two sine waves to a signal with only one sine wave. **f** Normally-distributed (Gaussian) noise with a stepwise transition in the mean and a change in the autocorrelation prior to this transition. The examples display the time series (upper panel), the recurrence plot (middle panel) and the RQA measures (lower panel). Embedding parameters m = embedding dimension, *tau* = time delay, e = threshold, w = window size, *ws* = window moving steps, *norm* = vector norm, *thei* = size of Theiler window, *lmin* = minimum line length, RQA measures *RR* = recurrence rate and *DET* = determinism. Please read the "Methods" section for a detailed description of the embedding parameters and RQA measures

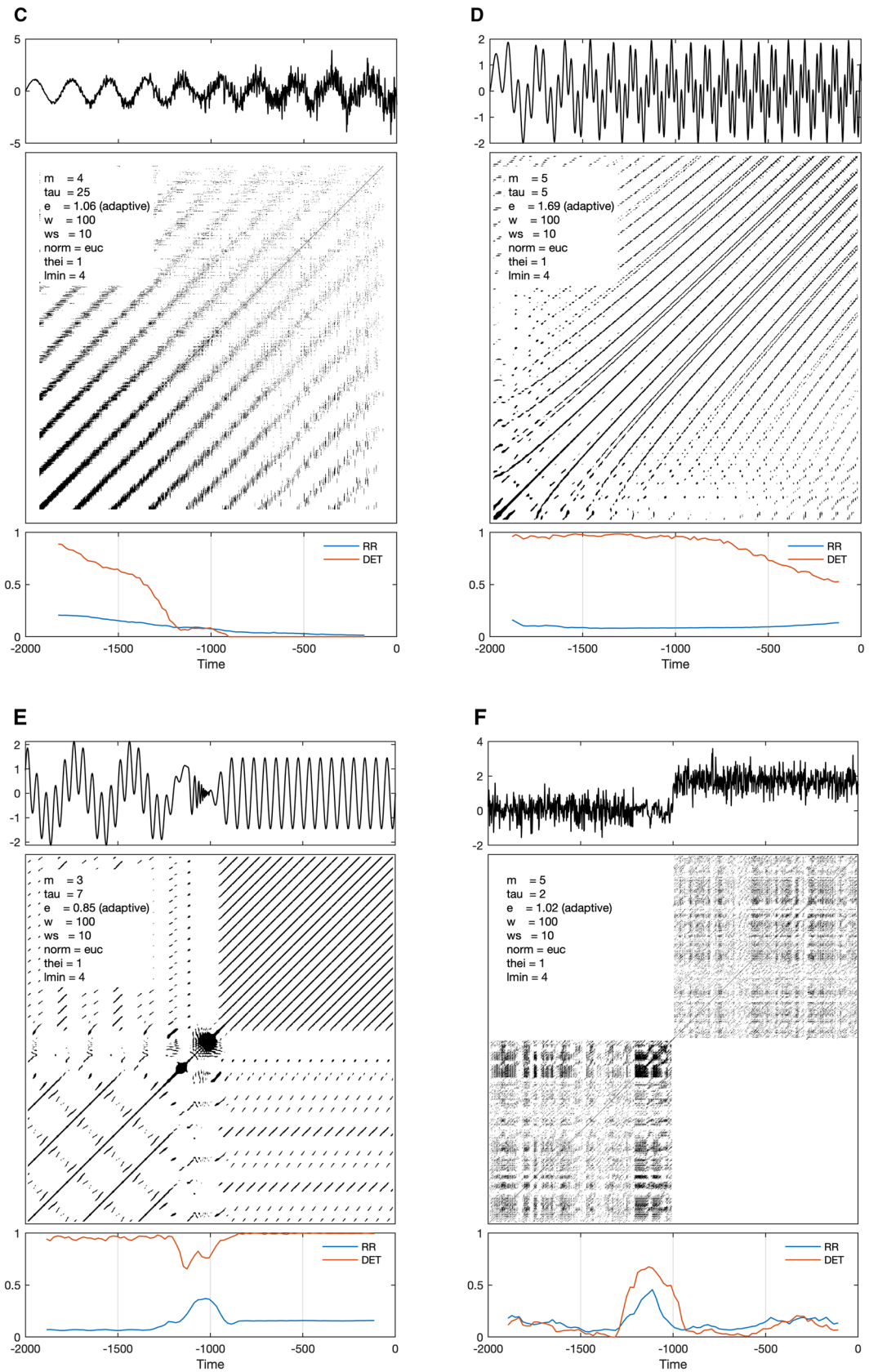

Fig. 3 (continued)

which is the density of black dots within the recurrence plot. This measure simply describes the probability of states of the system recurring within a particular time period.

Diagonal lines typically occur in recurrence plots when one segment of the trajectory runs almost parallel to another segment (e.g. within a given tolerance) representing an earlier episode in the history of the system within the phase space. Diagonal lines in recurrence plots are therefore diagnostic of cyclicity in time series; such cyclicity detected using recurrence plots is not restricted to sinusoidal structures, in contrast to cyclicity in Fourier-based time-series analysis. Cyclicity can be used to predict future conditions from present and past conditions using the ratio of the recurrence points that form diagonal patterns (of a certain length) to all other recurrence points, as a measure of the *determinism* (*DET*) or predictability of the system.

Misleading results can be obtained during analysis of the diagonal and vertical lines in recurrence plots due to what is known as tangential motion (Marwan et al. 2007). Tangential motion occurs when calculating points of recurrence if there are points in the phase space below the threshold value e that define the same trajectory segment, which is very typical of smooth or high resolution data (Marwan et al. 2007). This can lead to misleading RQA values, especially *DET* values. There are a number of methods that can be used to suppress this effect: (1) using a Theiler window defining the minimum time separation of nearest neighbors, (2) trailing data points on the phase space trajectory, or (3) by increasing the minimum length of the lines used to calculate the *DET* (Marwan et al. 2007). The latter method defines a lower limit for the length of the diagonal lines in order to exclude points on the same trajectory from *DET* calculations (Marwan et al. 2007; Marwan 2011).

RP analysis is further complicated by trends in the mean and variance (i.e. nonstationarity and long-term variations), which have a marked effect on the recurrence rate (*RR*), i.e. on the density of dots in RPs. If the long-scale variations are not of interest, the RQA characteristics can be used to reveal undesired fluctuations that do not reflect the more rapid variations in the dynamics of the system. We therefore use an adaptive threshold instead of a fixed value e, which is determined in such a way that all points in the phase space have the same number of neighbors. The *RR* is thus corrected for any changes in the density of points within the phase space. The resulting constant *RR*s (and hence more homogeneous RPs) make it easier to detect rapid changes of the system dynamics at a particular point, while long-term changes can be observed at other points. Note that the *RR* obtained by using an adaptive threshold is constant with respect to the whole RP and also to each column within the RP, since one column represents one point in time, hence one point in the (reconstructed) phase space. This means, we expect a time-dependent behavior of *RR*, when performing a windowed analysis over the entire RP and a constant *RR* with respect to the whole RP (see description below). One other possible problem in analyzing palaeoclimate records, which typically have very low signal-to-noise ratios, is the disruption of patterns in the RP (such as diagonal lines) by noise, gaps and other disturbances.

The RQA can be carried out using moving windows in order to detect changes in the system dynamics, represented by a change in the RQA measures, (1) by developing a single RP and calculating the RQA measures for windows moving along this RP, or (2) by developing multiple RPs of individual windows and calculating the RQA measures for these RPs. If nonstationarities (e.g. trends) are not the main focus of the analysis, then approach (2) makes it easier to find transitions while ignoring any nonstationarities. However, if the detection of overall changes is of interest (e.g. to test for nonstationarity), the recurrence conditions should be kept constant over time (thus taking into account the RP of the entire time series) and approach (1) will be more appropriate (Marwan 2011). A window size needs to be chosen that is small enough to ensure good temporal resolution but large enough to cover typical variations (e.g. the number of cycles) in order to be able to detect recurrences. Since our data show a very dominant long-term trend, we first perform the RQA on the original data and then on a high-pass filtered (and hence detrended) version of the data.

3.3 Synthetic examples of a recurrence quantification analysis

The investigation of synthetic data using RPs and the RQA measures described above, which are then used to analyse real data, has proven to be particularly advantageous when the methods are complex and the results not immediately obvious (e.g. Marwan et al. 2007; Trauth 2015) (Fig. 3). The use of conceptual models that mimic typical system changes helps us to understand the typical changes seen in RPs and to assign them to one or other of those changes. The first example investigated was of normally-distributed (Gaussian) noise, for which an RP and RQA measures were derived (Fig. 3a). The RP shows randomly distributed points, each representing times when the system randomly returned to a similar state. Similar states frequently recur in random noise but without any regularity except the states represented by the main diagonal line, the line of identity. The *RR* is therefore more or less constant with very low values. Since there is no systematic pattern (e.g. cyclically recurring states), the RP does not show any linear patterns and the *DET* is therefore very low.

The second example investigated was a composite signal of two sine waves, for which an RP and RQA measures were again derived. In the interval between − 1400 and − 600 there is a positive trend in the mean (Fig. 3b).

The RP shows long diagonal lines, diagnostic of cyclicity in time series, with shorter lines in between. The horizontal distances between these lines corresponds to the periods of the two sine waves ($T1 = 50$ and $T2 = 200$). Since the higher frequency is a harmonic of the lower frequency, the corresponding diagonal lines appear thicker in the RP. The RP clearly shows the effect of the trend in the mean as the diagonal lines disappear towards the upper left and lower right corners of the RP due to the trend-induced increase in the distance, leaving a blocky pattern in the middle of the RP. Because the dynamic itself does not change, neither do the *DET* values; instead they persist at their maximum values, which are unaffected by the trend. The *RR* is however affected, as shown by the lower density of black dots in the RP, indicating cyclic variations with a period of the same order as the dominant period in the signal ($T2 = 200$).

The synthetic data in the third example comprised a sine wave and Gaussian noise with a signal-to-noise ratio that decreases from left to right (Fig. 3c). As a result the continuity of the diagonal lines decreases to the right, as do both the *DET* and the *RR* values. The synthetic data in the fourth example investigated comprised a composite signal from two sine waves with distinct trends in their frequencies (Fig. 3d). The distances between diagonal lines decrease as a result of increasing signal compression with time. The convergence of the lines and their degree of curvature depend on the function describing the signal compression. The increase in frequency with time results in reductions in the *DET* because the higher-frequency cycles seen on the right of the plot are no longer adequately resolved. Recurrence points in between diagonal lines are scarce due to the fact that the time delay τ chosen for the plot no longer suits the increased frequency. A higher sampling rate eliminates this phenomenon.

The results of the fifth example revealed how RPs and RQAs respond to an abrupt transition from a composite signal consisting of two sine waves ($T1 = 300$, $T2 = 50$) to a signal with only one sine wave ($T3 = 60$) (Fig. 3e). As before, the oscillations of the signal produce diagonal lines in the RP, with horizontal distances between the lines corresponding to the periods of the signals. Two sets of diagonal lines in the lower-left corner of the RP correspond to the two frequencies of the sine waves, while there is only one set of diagonals in the upper right corner. During the transition we also let the amplitude of the signal decrease. Both the change from two sine waves to a single sine wave and the decrease in variance during the transition are clearly visible in the RP, as well as in the RQA measures. The single period oscillation has more recurrences than the two-period signal and therefore a higher *RR*, peaking at the transition because the lower signal variance produces a blocky pattern in the RP.

Because of the two different time scales of the two-period signal it has a more complicated phase-space trajectory on the left-hand side of the RP than the one-period signal. Trajectory segments are therefore only parallel at particular times, resulting in long diagonals for the long period signal (because $T2$ is a harmonic of $T1$, as in the second example above), but interrupted diagonals (and lines that are curved at times) for the short period signal. This results in slightly lower *DET* values before the transition to a one-period signal than after it. An effect similar to that seen in our third example is observed in the interval between $t = -1200$ and $t = -1050$ (where the actual transition from a two period signal to a one period signal occurs), which is why the *DET* decreases here before again increasing due to the blocky pattern in the RP, which also causes the *RR* to increase, as mentioned previously.

The synthetic data in the sixth example investigated was of Gaussian noise with a stepwise transition in the mean and a change in the autocorrelation prior to this transition (Fig. 3f). It is important to note that neither the mean nor the variances change in the pre-transition section, so this change cannot be recognized using conventional methods. The two blocky features in the RP before and after the transition look very similar to those in the RP of the first example above. However, the interval between − 1200 and − 1000 clearly shows distinctive patterns within the RP that are different from those typically occurring in RPs of pure noise. White vertical lines help to define blocky features that represent episodes with different dynamics. The RQA characteristics look similar to those in the Gaussian noise example except for a section with higher autocorrelation, which is reflected in the higher density of black dots, clear diagonal lines, and a change in the dynamics of the system. This fact can be used to detect such a change in autocorrelation as a precursor to a tipping point and to ultimately predict the tipping point itself.

4 Results

We have used recurrence plots (RPs), complemented by a recurrence quantification analysis (RQA), to characterize past climate change in the Chew Bahir basin over approximately the last 45 kyrs. We selected the *RR* and *DET* measures because they describe fundamental properties of the complex Chew Bahir system dynamics, while keeping the theoretical complexity within reasonable limits to facilitate interpretations. The RP and RQA approach was applied to the record of K concentrations in the sediment cores (following DTW-based alignment and linear unmixing using a PCA), which has previously been shown to be a reliable proxy for aridity in the Chew Bahir basin (Foerster et al. 2012, 2018; Trauth et al. 2015, 2018). The K record was embedded in phase spaces with dimensions varying from $m = 5$ to $m = 6$ and temporal distances varying from $\tau = 3$ to $\tau = 10$ data points, equivalent to 3×10 yrs $= 30$ yrs and

10×10 yrs $= 100$ yrs, where 10 yrs is the resolution of the time series following interpolation. The RPs were calculated using a Euclidean norm, a Theiler window of $thei = 1$ data point, a minimum length of $lmin = 3$ for the lines used to calculate *DET*, and an adaptive threshold value *e* rather than a fixed value. The size *w* and the step size *ws* of the moving window depend on the period of time investigated and the number of data points contained therein.

In order to compare different climatic conditions we first looked at the RP of the complete, unfiltered time series documenting the long-term variations in the Chew Bahir system (Fig. 4). This RP reveals a clear division of the time series into sections of different lengths, indicated by square blocky features in the RP separated by white vertical lines (see also Fig. 3b, e, f). The first cluster of recurrence points occurs between 45.35 and 37 kyr BP, comprising both connected and isolated points. This interval is characterized by both vertical and horizontal lines, representing episodes of stability (both wet and dry) interrupted by a series of extremely wet events, indicated by white vertical lines in the RP. We observe low but gradually increasing *DET* values in this episode, suggesting increasing predictability in the system.

A second, very obvious, cluster of recurrence points occurs between 37 and 20 kyr BP, which includes the time intervals in which the Dansgaard-Oeschger (DO) cycles (~ 110–23 kyr BP), the Heinrich Events (HE, ~ 60–12 kyr BP) and the Last Glacial Maximum (LGM, 23.5–18 kyr BP) affected the climate further to the north. The RQA reveals consistently high *DET* values until about 15 kyr BP, exceeding those of the previously described cluster and suggesting a much higher predictability in the system during that time. The recurrence plot for the time interval from 20 to 0 kyr BP includes the African Humid Period (AHP, ~ 15–5 kyr BP). This interval is characterized by three large clusters of recurrence points, interrupted by both white vertical and horizontal lines, together with fluctuating *RR* values and a long-term trend towards lower *DET* values. The white vertical lines again help to define blocky features marking episodes with different dynamics.

To analyze the dynamics of these individual sections, the time series was high-pass filtered with a cutoff frequency of 0.001 yrs^{-1} in order to remove any long-term trends (Figs. 5, 6, 7). An RP was constructed and an RQA performed using a sliding window ($w = 100$, $ws = 10$) over the

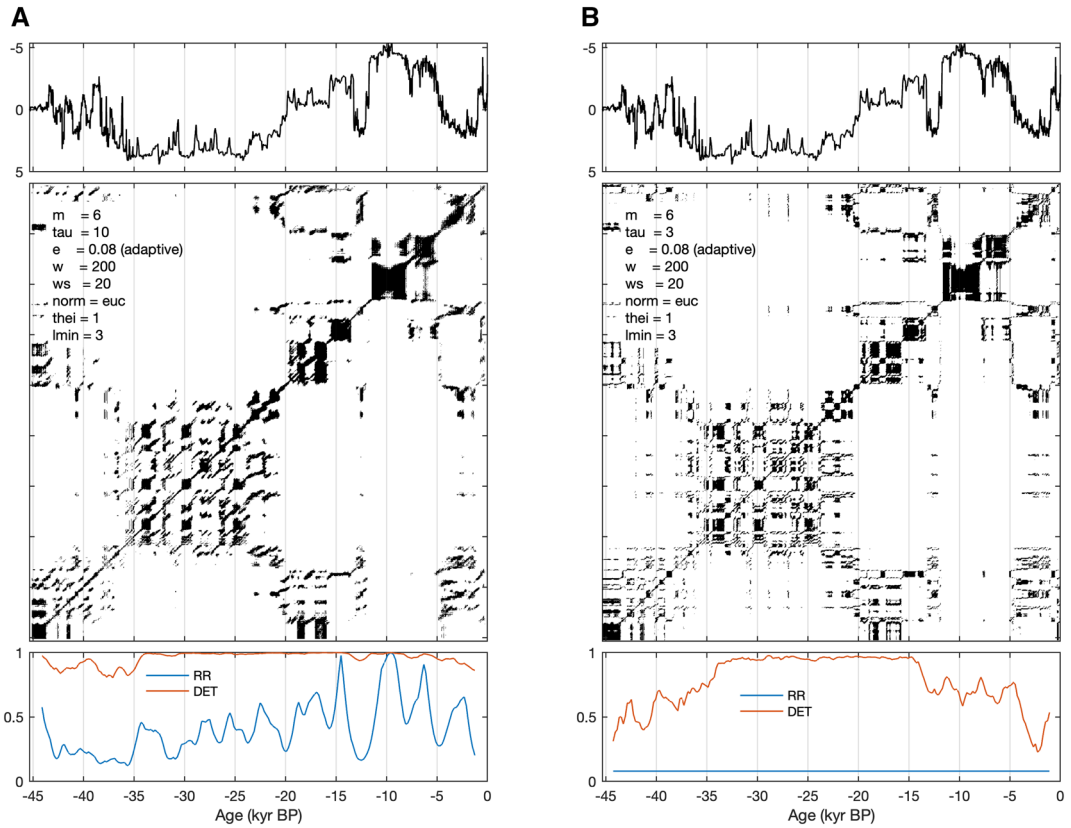

Fig. 4 Recurrence plot (RP) and recurrence quantification analysis (RQA) measures of the complete record (– 45,358 to 0 yrs BP) from the Chew Bahir basin: time series (upper panel), the recurrence plot (middle panel) and the RQA measures (lower panel) of moving windows determined either by **a** calculating the RQA measures for windows moving along a single (global) RP and **b** by calculating individual RPs for windows moving along the entire time series. See previous figure for the meaning of the abbreviations

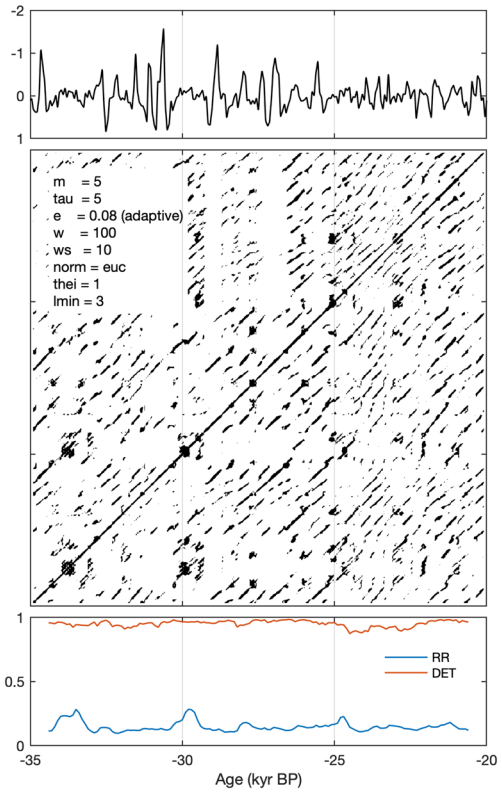

Fig. 5 Recurrence plot (RP) and recurrence quantification analysis (RQA) measures for the Chew Bahir basin covering of the time interval between 35 and 20 kyr BP: time series (upper panel), the recurrence plot (middle panel) and the RQA measures (lower panel) of moving windows determined by calculating individual RPs for windows moving along the entire time series. See previous figure for the meaning of the abbreviations

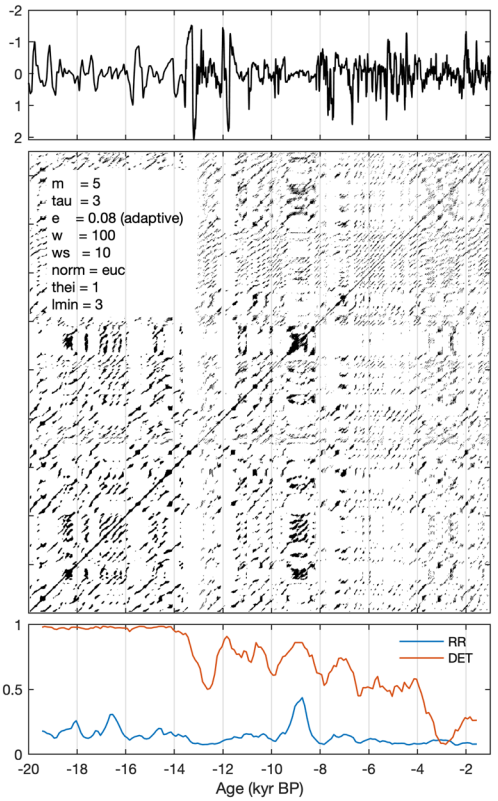

Fig. 6 Recurrence plot (RP) and recurrence quantification analysis (RQA) measures for the Chew Bahir basin covering of the time interval between 20 and 1 kyr BP: time series (upper panel), the recurrence plot (middle panel) and the RQA measures (lower panel) of moving windows determined by calculating individual RPs for windows moving along the entire time series. See previous figure for the meaning of the abbreviations

entire RP, assuming stationarity within the intervals. The interval between 35 and 20 kyr BP is remarkable for numerous short, slightly curved diagonal lines, suggesting a cyclic recurrence of wetter episodes in the Chew Bahir basin within a period that had a generally dry climate (Fig. 5). The oscillating climatic conditions are reflected in higher *DET* values, while the low *RR* values suggest a low probability of recurring states occurring within the system over a particular time period (Marwan et al. 2007).

The recurrence plot for the time interval from 20 to 1 kyr BP includes the AHP (~ 15–5 kyr BP) (Fig. 6). As before, using moving windows with a length of $w = 100$ (1000 yrs) and a step size of $ws = 10$ (100 yrs) reveals a series of blocky recurrence point patterns, interrupted by a series of white vertical lines. These patterns suggest distinct episodes of relative stability, both wet and dry, separated by abrupt transitions at ~ 13.2 kyr BP, ~ 11.8 kyr BP, ~ 7.5 kyr BP, ~ 5.2 kyr BP, and ~ 4.5 kyr BP. The overall appearance of the RP (and of the time series itself) reflects dynamics characterized by a period of higher variability followed by a period of low variability between 9.5 and 8 kyr BP, and dynamics dominated by a high-frequency cyclicity between 8 and 1 kyr BP, which is roughly similar to the fifth synthetic example above (see Fig. 3e). In addition to these patterns, the RP for the interval from 20 to 1 kyr BP also shows numerous short diagonal lines, suggesting a weak cyclicity. The diagonal lines, however, are very different from each other in width and in the number present. The *RR* values are very low except for an interval of relative stability between 10 and 8 kyr BP, which has a high probability of recurring states. The *DET* values document a general trend towards lower predictability in the system dynamics, but this decline exhibits a very complicated and somewhat cyclical pattern, rather than a simple linear trend.

In contrast to the RP for the first half of the time interval from 20 to 1 kyr BP, the RP for the period between 8 and 1 kyr BP contains numerous spotty diagonals following two blocky features at about 9 and 7 kyr BP (Fig. 7). These blocky features indicate a slowing-down of the system dynamics and therefore a higher predictability, as also indicated by high *DET* values (similar to the synthetic example

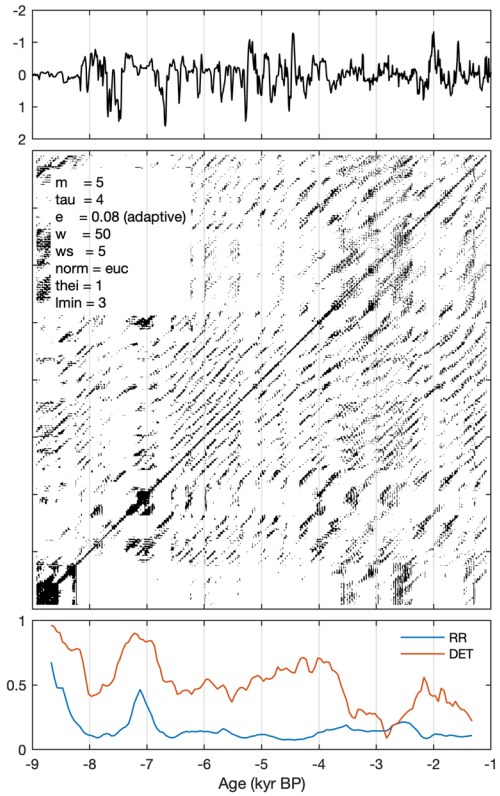

Fig. 7 Recurrence plot (RP) and recurrence quantification analysis (RQA) measures for the Chew Bahir basin of the time interval between 9 and 1 kyr BP: time series (upper panel), the recurrence plot (middle panel) and the RQA measures (lower panel) of moving windows determined by calculating individual RPs for windows moving along the time series. See previous figure for the meaning of the abbreviations

shown in Fig. 3e, f). The *RR* values are very low, except for one interval of relative stability. The distinctive diagonal lines after about 6.8 kyr BP suggest a marked cyclic recurrence of droughts approximately every 100–150 yrs, which lasted until stable conditions returned following the termination of the AHP. The relatively low *DET* values (~ 0.5) and therefore low predictability during this interval, however, reflects the discontinuity in the diagonal lines and the dispersion of cycles (i.e. the variability in distances between the diagonal lines, similar to the synthetic example shown in Fig. 3c, d), suggesting that a stochastic process is superimposed on the cyclicity. The *DET* values during the wet-dry transition at the end of the AHP remain moderately high in the high-pass filtered time series until stable dry conditions are established. The interval between 4 and 2 kyr BP with very low *DET* values (< 0.5) reflects a predominantly stochastic process.

5 Discussion

A section-by-section analysis of the RPs of the time series together with an examination of the temporal course of the RQA measures allows us to identify and eventually classify different types of variability and transitions (Table 1). The classification of variability and transitions can help to improve our understanding of the response of the biosphere (including humans) to climate changes (e.g. Donges et al. 2011; Foerster et al. 2015, 2018; Trauth et al. 2015, 2018). There is a general consensus amongst anthropologists that both long-term trends and severe, abrupt changes resulted in significant changes to the social and socio-economic behavior of early humans (Gatto and Zerboni 2015; Clark et al. 2016; Lahr 2016; Flohr et al. 2016). The response to a changing habitat, both subtle or dramatic, accompanied by changes in essential resources such as food and water, could be either expansion, decease,

Table 1 Compilation of the most important time periods in the Chew Bahir sediment cores, classified according to main climate, environmental conditions, recurrence plot appearance, recurrence rate RR, determinism DET, occurrence of extreme events and human habitat

Age (kyr)	45–37	37–20	20–16	16–10	10–8	8–4	4–now
Main climate	Intermediate	Dry	Intermediate	Wet, with YD dry event	Wet	Wet	Dry
Environmental conditions	Wet–dry trend	1500 yrs cycles	Long-term sinusoidal dry-wet-dry trend due to 20 kyr precession cycle			Stable with 160 yrs cycles	Stable, wet at the end
RP appearance	Irregular	Regular	Regular	Irregular	Regular	regular	Regular
Recurrence rate (RR)	Low	Intermediate	Intermediate	High, with low YD event	High	high	Intermediate
Determinism (DET)	Low	High	High	Intermediate	Intermediate	intermediate	Low
Extreme events	Random wet	Wet–dry	None	YD dry event	Possibly 8.2 kyr dry event	~14 dry events, 20–80 yrs long	Very arid, possibly wet after 2 kyr BP
Human habitat	Extreme radom wet events	Wet–dry cycles	Stable	Threshold	Stable, except for 8.2 kyr event	Threshold and cycles	Aridity

migration, or adaption (e.g. Foerster et al. 2015, 2018). In this process, the nature of the adaptation is a function of the adaptability and the time scale (e.g. Foerster et al. 2015, 2018). Of particular interest is how the adaptability of humans has enabled them to deal with such diverse and profound environmental changes since 45 kyrs BP through behavioral changes, and what level of environmental change met the limit of resilience (e.g. Marshall and Hildebrand 2002; Foerster et al. 2015, 2018; Trauth et al. 2015, 2018). Furthermore, the different types of variability and transitions, and the corresponding response of the biosphere (including humans), will help to detect similar types of changes in the long (~ 280 m) sediment cores recently collected in the Chew Bahir basin within the Hominin Sites and Paleolakes Drilling Project (HSPDP) and to investigate whether or not these types are typical for and exclusive to the basin, as well as the response of the biosphere to these changes.

Our analysis clearly shows a number of different types of variability in the K record, separated by either gradual or rapid transitions. The first type of variability occurs between the beginning of the record (45 kyr BP) and about 35 kyr BP. Within this interval we observe a relatively low but gradually increasing predictability during times of relative stability (both wet and dry), interrupted by a series of extremely wet events. There is no cyclicity in this interval but rather an irregular pattern of different types of variability. Both the extreme events and the rapid transitions between episodes of relative (wet and dry) stability will certainly have had an impact on humans in the area, leaving them with a range of possible responses (adapt, migrate, starve) to a dramatically changing environment (e.g. Foerster et al. 2015, 2018; Trauth et al. 2015, 2018).

The second type of variability occurs between 35 and 20 kyr BP, with slightly different dynamics before and after 25 kyr BP. This interval is characterized by a millennial-scale climate variations during the last glacial cycle, which includes the time intervals in which the Dansgaard–Oeschger (DO) cycles (~ 110–23 kyr BP), the Heinrich Events (HE, ~ 60–12 kyr BP) and the Last Glacial Maximum (LGM, 23.5–18 kyr BP) affected the climate further to the north. This millennial-scale climate fluctuations are cyclic with minor variations in the period, as indicated by the slight curvature of the diagonals in the RP (see synthetic example shown in Fig. 3d), although this curvature could also suggest inaccuracies in the age model, rather than real variations in the cyclicity. The pronounced cyclicity is reflected in the RP and in the RQA measures by a very high predictability, but on time scales that are certainly not relevant to humans, because it is orders of magnitude longer than the lifetime of individual humans. However, the transitions between the dry and wet episodes were very rapid which has probably caused significant stress to human populations.

The third type of variability occurs between 16 and 10 kyr BP, including parts of the AHP (~ 15–5 kyr BP). During this interval we find episodes of relative stability, both wet and dry, separated by abrupt transitions at ~ 13.2 kyr BP and ~ 11.8 kyr BP. There is also evidence of a weak cyclicity with a general (but complicated) trend towards lower predictability. The onset of the AHP in the Chew Bahir area was relatively rapid (covering ~ 240 yrs, Trauth et al. 2018), which is in agreement with similar records from elsewhere, as a result of large-scale deglacial forcings (i.e. changes of Atlantic sea-surface temperatures causing meridional shifts of the African easterly jet and the monsoon belt, and changes in the atmospheric concentration of greenhouse gases causing changes in atmospheric temperatures, Shanahan et al. 2015). The onset and termination of the dry episode during the Younger Dryas (YD) were also rapid transitions (over less than 100 yrs, Trauth et al. 2018), again very similar to other sites in N and NE Africa (e.g. Shanahan et al. 2015; Trauth et al. 2018).

The climate variability within the AHP and the long-term transition that it represents clearly affected human communities and has fueled massive changes in the population size and structure such as the profound socio-economic transformations that have been documented for N and NE Africa (e.g. Marshall and Hildebrand 2002; Brooks 2006; Clark et al. 2016; Lahr 2016; Marchant et al. 2018). A well-studied example is provided by demographic reconstructions that have been made for the Saharan Holocene. These reconstructions show a temporal delay between the onset of humid conditions (based on sedimentary dust flux records) and human reoccupation of former desert areas, with associated societal changes seen as a response to the environmental changes (Manning and Timpson 2014; Gatto and Zerboni 2015; Clark et al. 2016).

Having adapted to the wet climate of the AHP, humans certainly had to cope with the very rapid transition towards extreme dryness at the onset of the YD dry episode. Highly mobile groups of hunter-gatherers responded to short-term arid pulses by vertical migration as documented by the settlement patterns in what are assumed to have been refuge areas such as the SW Ethiopian Highlands (e.g. Foerster et al. 2015). The YD is followed by a short interval of relative stability between 10 and 8 kyr BP, followed by a dry episode centered around 7.5 kyr BP. This event, which is synchronous with the prolonged pause in the Green Sahara conditions 8 kyrs ago (within the uncertainty of our age model, see Trauth et al. 2015), coincides with a temporary abandonment of sites previously occupied by Neolithic humans (Tierney et al. 2017).

The fourth type of variability occurs between 8 and 4 kyr BP. This interval includes the transition from the humid climate of the AHP to the subsequent dry climate. The termination of the AHP was a result of weaker, insolation-driven

forcing (and hence more complex and time-transgressive responses) than that which produced the DO cycles, the onset of the AHP, or the onset/termination of the YD dry episode (Shanahan et al. 2015). This was nevertheless compared to those produced by more subtle changes in orbital forcing, but certainly not abrupt compared to human time scales, i.e. human lifespan or a little more, as it continued for approximately 990 years (Trauth et al. 2018). The termination of the AHP occurred at different times in other areas, suggesting a strong influence of Indian Ocean SSTs on the East African climate (Shanahan et al. 2015). Most of the transition at the end of the AHP is characterized by wet conditions, interrupted by at ~ 14 dry events that have recurred every 160 ± 40 years and lasted 20–80 years (Trauth et al. 2015). Compared to the low-frequency cyclicity of climate variability during the DO cycles, this type of cyclicity occurs on time scales equivalent to a few human generations. In other words, it is very likely (albeit speculative) that people were conscious of these changes and adapted their lifestyles to the consequent changes in water and food availability (Marshall and Hildebrand 2002; Clark et al. 2016).

An interesting aspect of this variability is the nature of the transitions close to the threshold in the system response, and how the environment switches from one stable mode to another. A rapid change of climate in response to a relatively modest change in forcing appears to be typical of tipping points in complex systems such as the Chew Bahir basin (Lenton et al. 2008; Ditlevsen and Johnsen 2010). If this is the case then the 14 dry events at the end of the AHP could represent precursors of an imminent tipping point that would have allowed a prediction of climate change in the Chew Bahir basin at that time. A deeper analysis of our data is however required to understand whether the wet-dry climate transition in the area was due to a saddle-node bifurcation in the structural stability of the climate, or whether it was induced by a stochastic fluctuation (Lenton et al. 2008; Ditlevsen and Johnsen 2010). The time interval after the termination of the AHP (< 4 kyr BP) leads into present-day conditions in the Chew Bahir basin.

6 Conclusions

We have used a recurrence quantification analysis (RQA) on environmental records from short cores collected during a pilot study within the Chew Bahir basin to characterize the Chew Bahir palaeolake as a dynamical system composed of interacting components. The different types of variability and transitions in these records were classified to improve our understanding of the response of the biosphere to climate change, and especially the response of humans in the area. This classification and the corresponding responses of the biosphere will enable the detection of similar types of variability and transitions in the long (~ 280 m) ICDP core collected in the Chew Bahir basin within the Hominin Sites and Paleolakes Drilling Project (HSPDP) and allow us to investigate whether or not these types are typical for and exclusive to the basin.

Acknowledgements Our project was funded by the DFG priority program SPP 1006 ICDP to M.H.T. and F.S. as well as the CRC 806 "Our Way to Europe" to F.S. at the University of Cologne. The project also received funds from a DFG grant to N.M. and M.H.T. to improve the recurrence plots/recurrence quantification analysis methods. This paper is publication number 19 of the Hominin Sites and Paleolakes Drilling Project (HSPDP). The MATLAB code to calculate the RPs and to perform the RQA is available at http://mres.uni-potsdam.de and on request from the corresponding author.

References

Ambrose SH (1998) Late Pleistocene human population bottlenecks, volcanic winter, and the differentiation of modern humans. J Hum Evol 35:115–118. https://doi.org/10.1006/jhev.1998.0219

Berke MA, Johnson TC, Werne JP, Livingstone DA, Grice K, Schouten S, Sinninghe Damsté JS (2014) Characterization of the last deglacial transition in tropical East Africa: insights from Lake Albert. Palaeogeogr Palaeoclimatol Palaeoecol 409:1–8

Brandt SA, Fisher EC, Hildebrand EA, Vogelsang R, Ambrose SH, Lesur J, Wang H (2012) Early MIS 3 occupation of Mochena Borago Rockshelter, Southwest Ethiopian highlands: implications for Late Pleistocene archaeology, paleoenvironments and modern human dispersals. Quatern Int 274:38–54. https://doi.org/10.1016/j.quaint.2012.03.047

Brooks N (2006) Cultural responses to aridity in the Middle Holocene and increased social complexity. Quatern Int 151:29–49. https://doi.org/10.1016/j.quaint.2006.01.013

Brown ET, Johnson TC, Scholz CA, Cohen AS, King JW (2007) Abrupt change in tropical African climate linked to the bipolar seesaw over the past 55,000 years. Geophys Res Lett 34:L20702. https://doi.org/10.1029/2007GL031240

Builes-Jaramillo A, Marwan N, Poveda G, Kurths J (2018) Nonlinear interactions between the Amazon River basin and the Tropical North Atlantic at interannual timescales. Clim Dyn 50:2951–2969. https://doi.org/10.1007/s00382-017-3785-8

Campisano CJ, Cohen AS, Arrowsmith JR, Asrat A, Behrensmeyer AK, Brown ET, Deino AL, Deocampo DM, Feibel CS, Kingston JD, Lamb HF, Lowenstein TK, Noren A, Olago DO, Owen RB, Pelletier JD, Potts R, Reed KE, Renaut RW, Russell JM, Russell JL, Schäbitz F, Stone JR, Trauth MH, Wynn JG (2017) The Hominin Sites and Paleolakes Drilling Project: high-resolution paleoclimate records from the East African Rift System and their implications for understanding the environmental context of hominin evolution. PaleoAnthropology 2017:1–43. https://doi.org/10.4207/PA.2017.ART104

Carto SL, Weaver AJ, Hetherington R, Lam Y, Wiebe EC (2009) Out of Africa and into an ice age: On the role of global climate change in the late Pleistocene expansion of early modern humans out of Africa. J Hum Evol 56:139–151. https://doi.org/10.1016/j.jhevol.2008.09.004

Castañeda IS, Mulitza S, Schefuß E, Santos RAL, Damste JSS, Schouten S (2009) Wet phases in the Sahara/Sahel region and human expansion patterns in North Africa. Proc Natl Acad Sci 106:1–5. https://doi.org/10.1073/pnas.0905771106

Cheung WH, Senay GB, Singh A (2008) Trends and spatial distribution of annual and seasonal rainfall in Ethiopia. Int J Climatol 28:1723–1734. https://doi.org/10.1002/joc.1623

Clark J, Brooks N, Banning EB, Bar-Matthews M, Campbell S, Clare L, Cremaschi M, di Lernia S, Drake N, Gallinaro M, Manning S, Nicoll K, Philip G, Rosen S, Schoop UD, Tafuri MA, Weninger B, Zerboni A (2016) Climatic changes and social transformations in the Near East and North Africa during the 'long' 4th millennium BC: a comparative study of environmental and archaeological evidence. Quatern Sci Rev 136:96–121. https://doi.org/10.1016/j.quascirev.2015.10.003

Cohen A, Campisano C, Arrowsmith R, Asrat A, Behrensmeyer AK, Deino A, Feibel C, Hill A, Johnson R, Kingson J, Lamb H, Lowenstein T, Noren A, Olago D, Owen RB, Potts R, Reed K, Renaut R, Schäbitz F, Tiercelin JJ, Trauth MH, Wynn J, Ivory S, Brady K, O'Grady R, Rodysill J, Githiri J, Russell J, Foerster V, Dommain R, Rucina S, Deocampo D, Russell J, Billingsley A, Beck C, Dorenbeck G, Dullo L, Feary D, Garello D, Gromig R, Johnson T, Junginger A, Karanja M, Kimburi E, Mbuthia A, McCartney T, McNulty E, Muiruri V, Nambiro E, Negash EW, Njagi D, Wilson JN, Rabideaux N, Raub T, Sier MJ, Smith P, Urban J, Warren M, Yadeta M, Yost C, Zinaye B (2016) The hominin sites and Paleolakes drilling project: inferring the environmental context of human evolution from eastern African Rift Lake deposits. Sci Drill 21:1–16. https://doi.org/10.5194/sd-21-1-2016

Cuthbert MO, Gleeson T, Reynolds SC, Bennett MR, Newton AC, McCormack CJ, Ashley GM (2017) Modelling the role of groundwater hydro-refugia in East African hominin evolution and dispersal. Nat Commun 8:15696

Davidson A (1983) The Omo River project: reconnaissance geology and geochemistry of parts of Ilubabor, Kefa, Gemu Gofa and Sidamo. Ethiopian Inst Geol Surv Bull 2:1–89

de Ramos AMT, Zou Y, de Oliviera GS, Kurths J, Macau EEN (2018) Unveiling non-stationary coupling between Amazon and ocean during recent extreme events. Clim Dyn 50:767–776. https://doi.org/10.1007/s00382-017-3640-y

deMenocal P, Ortiz J, Guilderson T, Adkins J, Sarnthein M, Baker L, Yarusinsky M (2000) Abrupt onset and termination of the African Humid Period: rapid climate responses to gradual insolation forcing. Quatern Sci Rev 19:347–361. https://doi.org/10.1016/S0277-3791(99)00081-5

Ditlevsen PD, Johnsen SJ (2010) Tipping points: Early warning and wishful thinking. Geophys Res Lett 37:L19703. https://doi.org/10.1029/2010GL044486

Donges JF, Donner RV, Trauth MH, Marwan N, Schellnhuber HJ, Kurths J (2011) Nonlinear detection of paleoclimate-variability transitions possibly related to human evolution. Proc Natl Acad Sci 108:20423–20427. https://doi.org/10.1073/pnas.1117052108

Eckmann JP, Kamphorst SO, Ruelle D (1987) Recurrence plots of dynamical systems. Europhys Lett 5:973–977. https://doi.org/10.1209/0295-5075/4/9/004

Eroglu D, McRobie FH, Ozken I, Stemler T, Wyrwoll KH, Breitenbach SFM, Marwan N, Kurths J (2016) See-saw relationship of the Holocene East Asian-Australian summer monsoon. Nat Commun. https://doi.org/10.1038/ncomms12929

Feldhoff JH, Donner RV, Donges JF, Marwan N, Kurths J (2013) Geometric signature of complex synchronisation scenarios. Europhys Lett 102:30007. https://doi.org/10.1209/0295-5075/102/30007

Flohr P, Fleitmann D, Matthews R, Matthews W, Black S (2016) Evidence of resilience to past climate change in Southwest Asia: Early farming communities and the 9.2 and 8.2 ka events. Quatern Sci Rev 136:23–39. https://doi.org/10.1016/j.quascirev.2015.06.022

Foerster V, Junginger A, Langkamp O, Gebru T, Asrat A, Umer M, Lamb H, Wennrich V, Rethemeyer J, Nowaczyk N, Trauth MH, Schäbitz F (2012) Climatic change recorded in the sediments of the Chew Bahir basin, southern Ethiopia, during the last 45,000 year. Quatern Int 274:25–37. https://doi.org/10.1016/j.quaint.2012.06.028

Foerster V, Vogelsang R, Junginger A, Asrat A, Lamb HF, Schaebitz F, Trauth MH (2015) Environmental change and human occupation of southern Ethiopia and Northern Kenya during the last 20,000 year. Quatern Sci Rev 129:333–340. https://doi.org/10.1016/j.quascirev.2015.10.026

Foerster V, Deocampo DM, Asrat A, Günter C, Junginger A, Kraemer H, Stroncik NA, Trauth MH (2018) Towards an understanding of climate proxy formation in the Chew Bahir basin, southern Ethiopian Rift. Palaeogeogr Palaeoclimatol Palaeoecol 501:111–123. https://doi.org/10.1016/j.palaeo.2018.04.009

Garcin Y (2008) Comment on "Abrupt change in tropical African climate linked to the bipolar seesaw over the past 55,000 yr" by Brown, E. T, Johnson, T. C, Scholz, C. A, Cohen, A. S, and King, J. W. (2007). Geophys Res Lett 35:L04701. https://doi.org/10.1029/2007GL032399

Garcin Y, Deschamps P, Ménot G, de Saulieu G, Schefuß E, Sebag D, Dupont LM, Oslisly R, Brademann B, Mbusnum KG, Onana JM, Ako AA, Epp LS, Tjallingii R, Strecker MR, Brauer A, Sachse D (2018) Early anthropogenic impact on Western Central African rainforests 2,600 y ago. Proc Natl Acad Sci 115:3261–3266. https://doi.org/10.1073/pnas.1715336115

Gasse F (2000) Hydrological changes in the African tropics since the Last Glacial Maximum. Quatern Sci Rev 19:189–211. https://doi.org/10.1016/S0277-3791(99)00061-X

Gatto MC, Zerboni A (2015) Holocene supra-regional environmental changes as trigger for major socio-cultural processes in Northeastern Africa and the Sahara. African Archaeol Rev 32:301–333. https://doi.org/10.1007/s10437-015-9191-x

Goswami B, Marwan N, Feulner G, Kurths J (2013) How do global temperature drivers influence each other? A network perspective using recurrences. Eur Phys J Spec Top 222:861–873. https://doi.org/10.1140/epjst/e2013-01889-8

Hailemeskel A, Fekadu H (2004) Geological map of Yabello. Geological Survey of Ethiopia, Addis Ababa **(ISN 0000 0001 0674 8528)**

Hassen N, Yemane T, Genzebu W (1997) Geology of the Agere Maryam Area. Geological Survey of Ethiopia, Addis Ababa

Hildebrand E, Grillo K (2012) Early herders and monumental sites in eastern Africa: New radiocarbon dates. Antiquity 86:338–352. https://doi.org/10.1017/S0003598X00062803

Ivory SJ, Russell J (2018) Lowland forest collapse and early human impacts at the end of the African Humid Period at Lake Edward, equatorial East Africa. Quatern Res 89:7–20. https://doi.org/10.1017/qua.2017.48

Iwanski J, Bradley E (1998) Recurrence plot analysis: To embed or not to embed? Chaos 8:861–871. https://doi.org/10.1063/1.166372

Kantz H, Schreiber T (1997) Nonlinear time series analysis. Cambridge University Press, Cambridge. https://doi.org/10.1017/CBO9780511755798

Key RM (1988) Geology of the Sabarei area: degree sheets 3 and 4, with coloured 1:250 000 geological map and results of geochemical exploration (Report). Ministry of Environment and Natural Resources, Mines and Geology Dept., Nairobi, Kenya

Klein RG (1995) Anatomy, behavior, and modern human origins. J World Prehist 9:167–198. https://doi.org/10.1007/BF02221838

Klein RG, Steele TE (2013) Archaeological shellfish size and later human evolution in Africa. Proc Natl Acad Sci 110:10910–10915. https://doi.org/10.1073/pnas.1304750110

Lahr M (2016) The shaping of human diversity: filters, boundaries and transitions. Philos Trans R Soc B 371:20150241. https://doi.org/10.1098/rstb.2015.0241

Lamb HF, Bates CR, Bryant CL, Davies SJ, Huws DG, Marshall MH, Roberts HM (2018) 150,000-year palaeoclimate record from northern Ethiopia supports early, multiple dispersals of modern

humans from Africa. Sci Rep 8:1077. https://doi.org/10.1038/s41598-018-19601-w
Lenton TM, Held H, Kriegler E, Hall JW, Lucht W, Rahmstorf S, Schellnhuber HJ (2008) Tipping elements in the Earth's climate system. Proc Natl Acad Sci 105:1786–1796. https://doi.org/10.1073/pnas.0705414105
Maley J, Doumenge C, Giresse P, Mahé G, Philippon N, Hubau W, Lokonda MO, Tshibamba JM, Chepstow-Lusty A (2018) Late Holocene forest contraction and fragmentation in central Africa. Quatern Res 89:43–59. https://doi.org/10.1017/qua.2017.97
Manning K, Timpson A (2014) The demographic response to Holocene climate change in the Sahara. Quatern Sci Rev 101:28–35. https://doi.org/10.1016/j.quascirev.2014.07.003
Marchant R, Richer S, Boles O, Capitani C, Courtney-Mustaphi CJ, Lane PJ et al (2018) Drivers and trajectories of land cover change in East Africa: Human and environmental interactions from 6000 years ago to present. Earth Sci Rev 178:322–378. https://doi.org/10.1016/j.earscirev.2017.12.010
Marshall F, Hildebrand E (2002) Cattle before the crops: the beginnings of food production in Africa. J World Prehist 16:99–143. https://doi.org/10.1023/A:10199549
Marwan N (2008) A Historical Review of Recurrence Plots. European Physical Journal. Spec Top 164:3–12. https://doi.org/10.1140/epjst/e2008-00829-1
Marwan N (2011) How to avoid potential pitfalls in recurrence plot based data analysis. J Biofurcation Chaos 21:1003–1017. https://doi.org/10.1142/S0218127411029008
Marwan N, Kurths J (2015) Complex network based techniques to identify extreme events and (sudden) transitions in spatio-temporal systems. Chaos 25:097609. https://doi.org/10.1063/1.4916924
Marwan N, Trauth MH, Vuille M, Kurths J (2003) Comparing modern and Pleistocene ENSO-like influences in NW Argentina using nonlinear time series analysis methods. Clim Dyn 21:317–326. https://doi.org/10.1007/s00382-003-0335-3
Marwan N, Romano MC, Thiel M, Kurths J (2007) Recurrence plots for the analysis of complex systems. Phys Rep 438:237–329. https://doi.org/10.1016/j.physrep.2006.11.001
Marwan N, Schinkel S, Kurths J (2013) Recurrence plots 25 years later - Gaining confidence in dynamical transitions. Europhys Lett 101:20007. https://doi.org/10.1209/0295-5075/101/20007
Moore JM, Davidson A (1978) Rift structure in southern Ethiopia. Tectonophysics 46:159–173. https://doi.org/10.1016/0040-1951(78)90111-7
Mudelsee M (2014) Climate time series analysis: classical statistical and bootstrap methods, 2nd edn. Springer, New York. https://doi.org/10.1007/978-3-319-04450-7
Nicholson SE (2017) Climate and climatic variability of rainfall over eastern Africa. Rev Geophys 55:590–635. https://doi.org/10.1002/2016RG000544
Packard NH, Crutchfield JP, Farmer JD, Shaw RS (1980) Geometry from a time series. Phys Rev Lett 45:712–716. https://doi.org/10.1103/PhysRevLett.45.712
Renfrew C (2009) Situating the creative explosion: universal or local? In: Renfrew C, Morley I (eds) Becoming human: innovation in prehistoric material and spiritual culture. Cambridge University Press, Cambridge, pp 74–92 **(ISBN-13:978-0521734660)**
Richter J, Hauck T, Vogersang R, Widlock T, Le Tensorer JM, Schmid P (2012) "Contextual areas" of early Homo sapiens and their significance for human dispersal from Africa into Eurasia between 200 ka and 70 ka. Quatern Int 274:5–24. https://doi.org/10.1016/j.quaint.2012.04.017
Rodó X, Rodríguez-Arias MA (2006) A new method to detect transitory signatures and local time/space variability structures in the climate system: the scale-dependent correlation analysis. Clim Dyn 27:441–458. https://doi.org/10.1007/s00382-005-0106-4
Runge J, Heitzig J, Marwan N, Kurths J (2012) Quantifying causal coupling strength: a lag-specific measure for multivariate time series related to transfer entropy. Phys Rev E 86:061121. https://doi.org/10.1103/PhysRevE.86.061121
Runge J, Petoukhov V, Kurths J (2014) Quantifying the strength and delay of climatic interactions: the ambiguities of cross correlation and a novel measure based on graphic models. J Clim 27:720–739. https://doi.org/10.1175/JCLI-D-13-00159.1
Saji NH, Goswami BN, Vinayachandran PN, Yamagata T (1999) A dipole mode in the tropical Indian Ocean. Nature 401:360–363. https://doi.org/10.1038/43854
Segele ZT, Lamb PJ, Leslie LM (2009) Seasonal-to-interannual variability of Ethiopia/Horn of Africa Monsoon. Part I: associations of wavelet-filtered large-scale atmospheric circulation and global sea surface temperature. J Clim 22:3396–3421. https://doi.org/10.1175/2008JCLI2859.1
Seleshi Y, Zanke U (2004) Recent changes in rainfall and rainy days in Ethiopia. Int J Climatol 24:973–983. https://doi.org/10.1002/joc.1052
Shakun JD, Carlson AE (2010) A global perspective on Last Glacial Maximum to Holocene climate change. Quatern Sci Rev 29:1801–1816. https://doi.org/10.1016/j.quascirev.2010.03.016
Shanahan TM, McKay NP, Hughen KA, Overpeck JT, Otto-Bliesner B, Heil CW, King J, Scholz CA, Peck J (2015) The time-transgressive termination of the African Humid Period. Nat Geosci 8:140–144. https://doi.org/10.1038/NGEO2329
Takens F (1981) Detecting strange attractors in turbulence, Lecture Notes in Mathematics, vol 898. Springer, Berlin, pp 366–381. https://doi.org/10.1007/BFb0091924
Tierney JE, deMenocal PB (2013) Abrupt shifts in horn of Africa hydroclimate since the last glacial maximum. Science 342:843–846. https://doi.org/10.1126/science.1240411
Tierney JE, Pausata FSR, deMenocal PB (2017) Rainfall regimes of the Green Sahara. Sci Adv 3:e1601503. https://doi.org/10.1126/sciadv.1601503
Timmerman A, Friedrich T (2016) Late Pleistocene climate drivers of early human migration. Nature 538:92–95. https://doi.org/10.1038/nature19365
Trauth MH (2015) MATLAB recipes for earth sciences, 4th edn. Springer, New York **(ISBN: 978-3-662-46244-7)**
Trauth MH, Maslin MA, Deino A, Strecker MR, Bergner AGN, Dühnforth M (2007) High- and low-latitude forcing of Plio-Pleistocene African climate and human evolution. J Hum Evol 53:475–486. https://doi.org/10.1016/j.jhevol.2006.12.009
Trauth MH, Bergner AGN, Foerster V, Junginger A, Maslin MA, Schaebitz F (2015) Episodes of environmental stability and instability in late Cenozoic lake records of Eastern Africa. J Hum Evol 87:21–31. https://doi.org/10.1016/j.jhevol.2015.03.011
Trauth MH, Foerster V, Junginger A, Asrat A, Lamb HF, Schaebitz F (2018) Abrupt or gradual? Change point analysis of the late Pleistocene-Holocene climate record from Chew Bahir, southern Ethiopia. Quatern Res 90:321–330. https://doi.org/10.1017/qua.2018.30
Tsonis AA (2018) Advances in nonlinear geosciences. Springer, New York **(ISBN: 978-3-319-58894-0)**
Turcotte DL (2010) Fractals and Chaos in geology and geophysics. Cambridge University Press, Cambridge. https://doi.org/10.1017/CBO9781139174695
Vogelsang R, Keding B (2013) Climate, culture, and change: From hunters to herders in northeastern and southwestern Africa. In: Comparative Archaeology and Paleoclimatology—Socio-cultural responses to a changing world, Baldia MO, Perttula TK, Frink

DS, eds.), BAR International Series, 2456, Archaeopress, Oxford, UK, pp 43–62

Webber CL, Zbilut JP (2005) Recurrence quantification analysis of nonlinear dynamical systems. In: Riley MA, Van Orden GC (eds) Tutorials in contemporary nonlinear methods for the behavioral sciences. http://www.saistmp.com/publications/spiegorqa.pdf. https://doi.org/10.1007/978-3-319-07155-8

Zbilut JP, Webber CL Jr (1992) Embeddings and delays as derived from quantification of recurrence plots. Phys Lett A 171:199–203. https://doi.org/10.1016/0375-9601(92)90426-M